

Molecular detection of SARS-CoV-2 in formalin-fixed, paraffin-embedded specimens

Jun Liu,¹ April M. Babka,¹ Brian J. Kearney,¹ Sheli R. Radoshitzky,¹ Jens H. Kuhn,² and Xiankun Zeng¹

¹United States Army Medical Research Institute of Infectious Diseases (USAMRIID), Fort Detrick, Frederick, Maryland, USA. ²Integrated Research Facility at Fort Detrick, National Institute of Allergy and Infectious Diseases (NIAID), NIH, Fort Detrick, Frederick, Maryland, USA.

Severe acute respiratory syndrome coronavirus 2 (SARS-CoV-2), the cause of human coronavirus disease 2019 (COVID-19), emerged in Wuhan, China, in December 2019. The virus rapidly spread globally, resulting in a public health crisis including almost 5 million cases and 323,256 deaths as of May 21, 2020. Here, we describe the identification and evaluation of commercially available reagents and assays for the molecular detection of SARS-CoV-2 in infected FFPE cell pellets. We identified a suitable rabbit polyclonal anti-SARS-CoV spike protein antibody and a mouse monoclonal anti-SARS-CoV nucleocapsid protein (NP) antibody for cross-detection of the respective SARS-CoV-2 proteins by IHC and immunofluorescence assay (IFA). Next, we established RNAscope in situ hybridization (ISH) to detect SARS-CoV-2 RNA. Furthermore, we established a multiplex FISH (mFISH) to detect positive-sense SARS-CoV-2 RNA and negative-sense SARS-CoV-2 RNA (a replicative intermediate indicating viral replication). Finally, we developed a dual staining assay using IHC and ISH to detect SARS-CoV-2 antigen and RNA in the same FFPE section. It is hoped that these reagents and assays will accelerate COVID-19 pathogenesis studies in humans and in COVID-19 animal models.

Introduction

Severe acute respiratory syndrome coronavirus 2 (SARS-CoV-2), the etiologic agent of human coronavirus disease 2019 (COVID-19), initially emerged in Wuhan, Hubei Province, China, in December 2019 (1–3). As of May 21, 2020, 4,893,186 cases of COVID-19, including 323,256 deaths, have been reported worldwide (4).

SARS-CoV-2 has a nonsegmented, linear, positive-sense, multicistronic genome and produces enveloped virions (5). The virus is classified as a betacoronavirus (*Nidovirales: Coronaviridae*) together with the other 2 highly virulent human pathogens severe acute respiratory syndrome coronavirus (SARS-CoV) and Middle East respiratory syndrome coronavirus (MERS-CoV) (6). The SARS-CoV-2 genomes shares 79.6% and 50.0% nucleotide sequence identity with the genomes of SARS-CoV and MERS-CoV, respectively (5). Similar to SARS-CoV, SARS-CoV-2 virions use their spike (S) glycoproteins to engage host-cell angiotensin I-converting enzyme 2 (ACE2) to gain entry into host cells and host-cell transmembrane serine protease 2 (TMPRSS2) for S priming (7).

Bats are speculated to be the natural reservoir of SARS-CoV-2 because numerous other betacoronaviruses are of chiropteran origin (8, 9). However, although the COVID-19 pandemic may have begun with a bat-to-human transmission event, it appears that nearly all human infections trace back to respiratory droplets produced by infected people and fomites (respiratory droplet landing sites) (10, 11). Human infections lead to various degrees of disease severity, ranging from asymptomatic infection or mild symptoms to fatal pneumonia. Older patients or patients with chronic medical conditions are more vulnerable to becoming critically ill with poor prognosis (12). The most common symptoms and clinical signs of COVID-19 are fever, cough, dyspnea, and myalgia, with a median incubation period of 4 days (13–15). Ground-glass opacity is the most common radiologic finding on chest CT upon admission (13–15). Bilateral diffuse alveolar damage, alveolar hemorrhage and edema, interstitial fibrosis and inflammation, and type II pneumocyte hyperplasia are observed in postmortem human lungs (16–18).

Conflict of interest: The authors have declared that no conflict of interest exists.

Copyright: © 2020, American Society for Clinical Investigation.

Submitted: April 10, 2020

Accepted: May 6, 2020

Published: June 18, 2020.

Reference information: *JCI Insight*. 2020;5(12):e139042.
<https://doi.org/10.1172/jci.insight.139042>.

At the time of writing, there were no animal models that truly mimic the disease spectrum and pathogenesis of COVID-19. However, small animals — for example, human ACE2-transgenic laboratory mice (19), cats (20), domestic ferrets (20, 21), golden hamsters (22), and nonhuman primates (e.g., rhesus monkeys, refs. 23, 24; crab-eating macaques, ref. 25) — are used to study SARS-CoV-2 infection, as alveolar damage, interstitial inflammation, and viral shedding occur in these animal models to various degrees. It is hoped that further development of these and establishment of other animal models will help overcome the current roadblock to evaluating the efficacy of candidate medical countermeasures (MCMs) against and the pathogenesis of COVID-19.

Detection of viral antigen using IHC or immunofluorescence assay (IFA) techniques and detection of viral nucleic acids using *in situ* hybridization (ISH) within infected, but inactivated, human or animal model tissues greatly facilitate detection of viral infection and thereby pathogenesis and MCM efficacy studies. These techniques become paramount in particular for studies of a potential pathogen that does not cause overt, or causes only mild, disease, such as SARS-CoV-2 in the currently available animal models. Viral antigen-based immunostaining has been used to detect SARS-CoV-2 antigen in both postmortem human and animal tissues (1, 16, 22, 25). However, the antibodies used in these studies were produced in-house and therefore are not commonly available. Identification and characterization of commercially available anti-SARS-CoV-2 antibodies and ISH assays that can be used to detect SARS-CoV-2 in FFPE tissues are therefore critically needed.

Here, we describe the evaluation of a rabbit polyclonal anti-SARS-CoV S antibody and a mouse monoclonal anti-SARS-CoV nucleocapsid protein (NP) antibody that are commercially available and, in IHC and IFA, recognized respective SARS-CoV-2 proteins in FFPE specimens. We also identify 2 commercially available ISH assays that can be used to efficiently detect SARS-CoV-2 RNA in such specimens and develop a dual staining assay using IHC and ISH to detect SARS-CoV-2 S and RNA in the same FFPE section.

Results

Identification of antibodies suitable for detection of SARS-CoV-2 by IHC and IFA in FFPE specimens. To identify antibodies that can be used to detect SARS-CoV-2 in human and animal tissues, we searched for commercially available SARS-CoV antibodies that recognize epitopes that are likely conserved in SARS-CoV-2. We identified 6 antibodies — including 3 rabbit polyclonal antibodies, against SARS-CoV S, 1 rabbit polyclonal antibody against SARS-CoV NP, and 1 rabbit and 1 mouse monoclonal antibody against SARS-CoV NP — that may cross-react with SARS-CoV-2 (Supplemental Table 1; supplemental material available online with this article; <https://doi.org/10.1172/jci.insight.139042DS1>). Additionally, we identified a rabbit monoclonal antibody against SARS-CoV-2 S (Supplemental Table 1). To evaluate whether these 6 antibodies can recognize SARS-CoV-2 in FFPE specimens, we performed IHC on FFPE pellets of Vero 76 cells infected with SARS-CoV-2. We identified 1 rabbit polyclonal antibody against SARS-CoV S (Sino Biological, 40150-T62-COV2) and a mouse monoclonal antibody against SARS-CoV NP (Sino Biological, 40143-MM05) that did not stain uninfected, but stained SARS-CoV-2-infected, FFPE cell pellets (Figure 1, A–D). Furthermore, we performed IFA using these 2 antibodies. Interestingly, in comparison to relatively concentrated detection of SARS-CoV-2 NP (red) in cytoplasmic membrane, SARS-CoV-2 S (green) was more confined in perinuclear inclusion bodies (Figure 1E).

Detection of SARS-CoV-2 RNA by ISH in FFPE tissues. We have previously reported the development of RNAscope ISH assays to detect various high-consequence viruses including Ebola virus (EBOV; *Filoviridae: Ebolavirus*), Marburg virus (MARV; *Filoviridae: Marburgvirus*), Lassa virus (LASV; *Arenaviridae: Mammarenavirus*), and Nipah virus (NiV; *Paramyxoviridae: Henipavirus*) in FFPE animal tissues (26–29). Here we used the RNAscope ISH assay to detect SARS-CoV-2 RNA in FFPE cell pellets using 3 probes: 2 binding the SARS-CoV-2 positive-sense (genomic) RNA and 1 binding the negative-sense (replicative intermediate) RNA (Figure 2, A–F, and Supplemental Table 2). As expected, the 40-ZZ positive-sense RNA probe 2 binding to SARS-CoV-2 positive-sense RNA resulted in a stronger signal than the 20-ZZ positive-sense RNA probe 1 (Figure 2, A–D). Interestingly, in contrast to the wide cytoplasmic distribution of SARS-CoV-2 positive-sense RNA (Figure 2, B and D), SARS-CoV-2 negative-sense (replicative intermediate) RNA, detected using negative-sense RNA probe 1, was more specifically localized in perinuclear inclusion bodies (Figure 2F).

Detection of SARS-CoV-2 replication in FFPE specimens using multiplex FISH. Single-stranded RNA viruses, such as SARS-CoV-2, have to generate a replicative intermediate RNA as a template to synthesize progeny genomic RNAs. We have previously reported the use of multiplex FISH (mFISH) to detect EBOV, MARV, and NiV replication in FFPE tissues (26, 28, 29). Here, we tested mFISH to detect

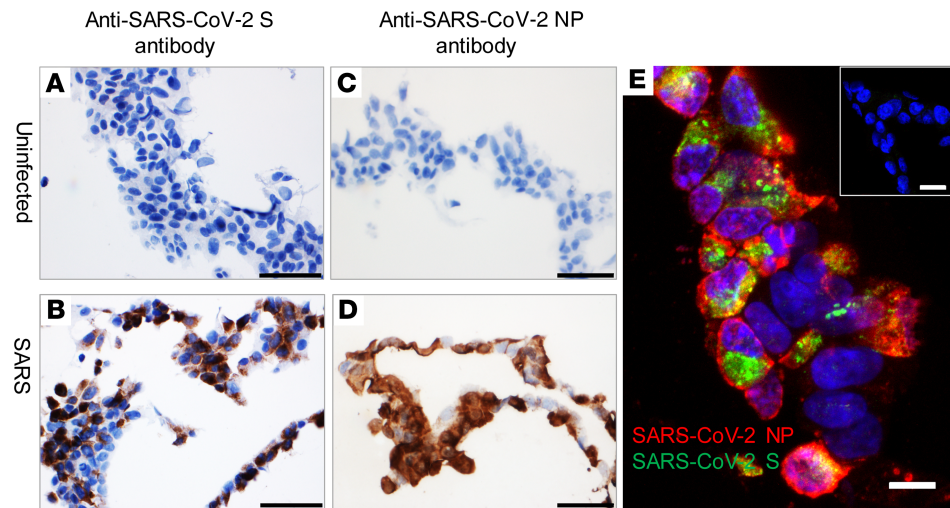


Figure 1. Detection of SARS-CoV-2 antigens by IHC and IFA in FFPE cell pellets. (A and B) In comparison to uninfected control FFPE cell pellets (A and C), SARS-CoV-2 S (brown, B) and SARS-CoV-2 NP (brown, D) can be detected in FFPE SARS-CoV-2-infected cell pellets. Nuclei are stained blue (hematoxylin). (E) Immunofluorescence staining to detect SARS-CoV-2 S (green) and NP (red) in FFPE SARS-CoV-2-infected cell pellets. Inset: Uninfected control FFPE cell pellets. Nuclei are stained blue (DAPI). Scale bars: 50 μ m in A–D; 20 μ m in inset of E; and 10 μ m in E.

SARS-CoV-2 replication in FFPE specimens using positive-sense RNA probe 2 and negative-sense RNA probe 2 (Supplemental Table 2). Consistent with the RNAscope ISH results, positive-sense viral RNA was widely distributed in the cytoplasm, whereas negative-sense RNA (replicative intermediate) was confined to perinuclear inclusion bodies (Figure 3, A and B).

Dual staining to detect SARS-CoV-2 antigen and RNA in the same FFPE section. To more precisely detect SARS-CoV-2, we developed a dual staining assay to recognize both SARS-CoV-2 antigen and RNA in the same FFPE section. IHC was performed using the identified rabbit polyclonal anti-SARS-CoV S antibody following ISH using positive-sense RNA probe 2. SARS-CoV-2 antigen was detected along with positive-sense RNA in the cytoplasm of most of the infected, but not in uninfected, cells (Figure 4, A and B).

Discussion

As infectious disease researchers worldwide are racing to understand the pathogenesis of and to develop and evaluate MCMs against COVID-19 to contain the ongoing pandemic, assays that determine SARS-CoV-2 distribution in tissues and specific cellular targets of infection are urgently needed. Here we evaluated commercial reagents and assays to detect SARS-CoV-2 antigens or RNA in FFPE specimens. We identified one rabbit polyclonal antibody and one mouse monoclonal antibody that react with SARS-CoV-2 S and NP, respectively, and demonstrated that these 2 antibodies can be used to detect SARS-CoV-2 by IHC and IFA in FFPE specimens. Additionally, we characterized 2 RNAscope ISH assays that can be used to detect SARS-CoV-2 positive- and negative-sense RNAs in FFPE specimens. Furthermore, we developed a dual staining assay using IHC and ISH to detect SARS-CoV-2 S and RNA in the same FFPE section. These reagents and assays are all commercially available and therefore can be applied readily to detect SARS-CoV-2 in both human and animal FFPE tissues.

IHC and IFA for viral antigens have been widely used to detect infection with high-consequence viruses, including SARS-CoV, EBOV, MARV, LASV, and NiV in human and animal FFPE tissues (26, 28–32). Although various antigen retrieval methods can help to restore the immunoreactivity of epitopes in FFPE tissues, in our experience it remains more challenging to identify antibodies that bind their targets in FFPE tissues compared with frozen section tissues. The FFPE specimen-compatible rabbit and mouse anti-SARS-CoV-2 antibodies we characterized here can be used to map the cellular targets of SARS-CoV-2 in various organs using multiplex IFA in addition to detecting viral infection. However, SARS-CoV-2-specific antibodies will have to be produced and characterized, because 2 antibodies we characterized here recognize both SARS-CoV and SARS-CoV-2 and may also cross-react with other coronaviruses. RNAscope ISH is a relatively novel ISH platform with high sensitivity and low background due to its unique ZZ probe design (33).

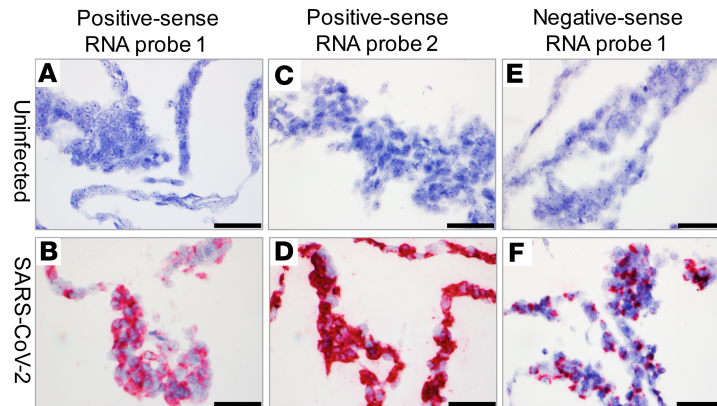


Figure 2. Detection of SARS-CoV-2 RNA by ISH in FFPE cell pellets. (A and B) SARS-CoV-2 positive-sense RNA can be detected by ISH using positive-sense RNA probe 1 in infected FFPE cell pellets (B), but not in uninfected control FFPE cell pellets (A). (C and D) SARS-CoV-2 positive-sense RNA can be detected by ISH using positive-sense RNA probe 2 in infected FFPE cell pellets (D), but not in uninfected control FFPE cell pellets (C). (E and F) SARS-CoV-2 negative-sense RNA can be detected by ISH using negative-sense RNA probe 1 in infected FFPE cell pellets (E), but not in uninfected control FFPE cell pellets (F). Nuclei are stained blue (hematoxylin). Scale bars: 50 μ m.

This platform has been widely used to detect viruses both in human and animal tissues (27, 34–36). Single-stranded RNA viruses have to produce a replicative intermediate, antigenomic RNA, as a template to synthesize new genomic RNAs. The presence of such replicative intermediate RNA in tissues indicates ongoing viral replication (26, 28, 29). The commercially available RNAscope ISH assays, including chromogenic and fluorescence assays, that we characterized here can be applied to detect viral RNA in both human and animal tissue samples. In contrast to detection of positive-sense (genomic) SARS-CoV-2 RNA, detection of negative-sense (replicative intermediate) RNA indicates active viral replication in cells or tissues at the time when the samples are collected. The perinuclear localization of negative-sense RNA detected by ISH we observed corresponds to the perinuclear localization of the coronavirus RNA replicase-transcriptase complex, which drives production of negative-sense RNAs through both replication and transcription, localized to intracellular membranes that are derived from the rough ER (37).

The dual staining we developed to detect SARS-CoV-2 viral antigen and RNA in the same FFPE section can more precisely detect SARS-CoV-2, because a positive IHC or ISH signal alone may originate from remaining free viral antigen or degenerating RNA fragments rather than from viral particles. Because SARS-CoV-2-infected animal tissues were not available at the time of this study, we were restricted to evaluating FFPE pellets of Vero 76 cells as a surrogate. However, we prepared FFPE cell pellets using the same process used for FFPE tissue preparation. Additionally, FFPE cell pellets have been widely used to evaluate antibodies, and ISH assays and other reagents for FFPE tissue analysis and have been largely predictive of reactivity with genuine tissues (33, 38, 39). Nevertheless, these assays must be further validated using human and animal tissues once they become widely available. We believe that the SARS-CoV-2 IHC, ISH, mFISH, and dual staining assays we developed and characterized will be useful for studying the pathogenesis of SARS-CoV-2 infection in both human and animal models.

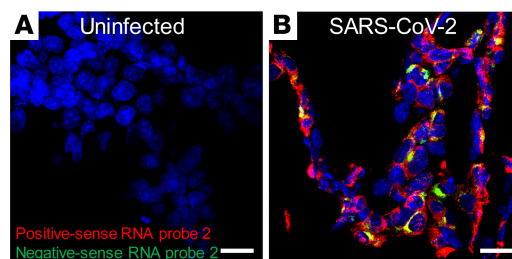


Figure 3. Detection of SARS-CoV-2 replication in FFPE cells using mFISH. (A and B) Compared with uninfected control (A), SARS-CoV-2 negative-sense RNA (green), a replicative intermediate that indicates viral replication, can be detected in infected FFPE cell pellets in addition to positive-sense (red) RNA (B). Nuclei are stained blue (DAPI). Scale bars: 20 μ m.

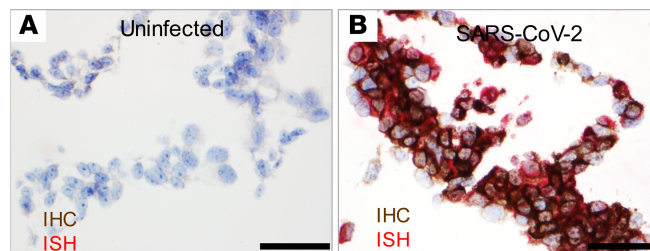


Figure 4. Dual staining to detect SARS-CoV-2 antigen and RNA in the same FFPE section. (A and B) Compared with uninfected control FFPE cell pellets (A), SARS-CoV-2 S (brown) and positive-sense RNA (red) were detected in the same section (B). Nuclei are stained blue (hematoxylin). Scale bars: 50 μm .

Methods

Cells and virus. Grivet (*Chlorocebus aethiops*) Vero 76 kidney epithelial cells (ATCC CRL-1587) were maintained in Eagle's minimum essential medium (EMEM; Thermo Fisher Scientific) supplemented with 10% heat-inactivated FBS (HyClone), 1% GlutaMAX (Thermo Fisher Scientific), and 1% non-essential amino acid solution (MilliporeSigma), at 37°C in a 5% CO₂ atmosphere. The SARS-CoV-2 USA-WA1/2020 strain (GenBank MN985325.1) was obtained from the CDC. Virus was added to Vero 76 cell cultures in T-75 flasks in biosafety level 3 (BSL-3) containment at an MOI of 0.01. Cells were then incubated for 1 hour for virus adsorption, washed with EMEM, and maintained in EMEM with 10% FBS. Cells were fixed at 24 hours after inoculation in 10% neutral buffered formalin for 24 hours, then moved from the BSL-3 to a BSL-2 suite. Uninfected Vero 76 cells were processed as a control.

Cell pellet embedding. Fixed cells were scraped off flasks after being rinsed twice in PBS (Thermo Fisher Scientific). Scraped cells were spun down at 140 g, and the pellets were mixed with liquefied HistoGel (Thermo Fisher Scientific). Pellets were solidified at 4°C and further processed for paraffin embedding using an automated Tissue-Tek VIP processor (Sakura).

IHC. IHC was performed using the EnVision system (Dako Agilent Pathology Solutions). Briefly, after deparaffinization, peroxidase blocking, and antigen retrieval, sections were covered with a primary antibody at a 1:1000, 1:2000, or 1:4000 dilution (Supplemental Table 1) and incubated at room temperature for 45 minutes. Subsequently, sections were rinsed, and the peroxidase-labeled polymer (secondary antibody) was applied for 30 minutes. Slides were rinsed, and a brown chromogenic substrate DAB solution (Dako Agilent Pathology Solutions) was applied for 8 minutes. The substrate-chromogen solution was rinsed off the slides, and slides were counterstained with hematoxylin and rinsed. The sections were dehydrated, cleared with Xyless II (Valtech), and coverslipped.

IFA. After deparaffinization and reduction of autofluorescence, tissues were heated in citrate buffer, pH 6.0 (MilliporeSigma), for 15 minutes to reverse formaldehyde cross-links. After rinsing with PBS, pH 7.4 (Thermo Fisher Scientific), sections were blocked overnight with CAS-Block (Thermo Fisher Scientific) containing 5% normal goat serum (MilliporeSigma) at 4°C. Sections were then incubated with rabbit polyclonal antibody against SARS-CoV S (Sino Biological, 40150-T62-COV2) at 1:500 dilution and mouse monoclonal antibody against SARS-CoV NP (Sino Biological, 40143-MM05) at 1:500 dilution for 2 hours at room temperature. After rinsing in PBST (PBS plus 0.1% Tween-20; MilliporeSigma), sections were incubated with secondary goat IgG Alexa Fluor 488-conjugated anti-rabbit antibody and with goat IgG Alexa Fluor 561-conjugated anti-mouse antibody (Thermo Fisher Scientific) for 1 hour at room temperature. Sections were coverslipped using VECTASHIELD antifade mounting medium with DAPI (Vector Laboratories). Images were captured on an LSM 880 confocal microscope (Zeiss) and processed using ImageJ (NIH).

ISH. To detect SARS-CoV-2 genomic RNA in FFPE tissues, ISH was performed using the RNAscope 2.5 HD RED kit (Advanced Cell Diagnostics) according to the manufacturer's instructions. Briefly, 40-ZZ ISH probes (catalog 854841, positive-sense RNA probe 1) with C1 channel and 20-ZZ ISH probes (848561, positive-sense RNA probe 2) with C1 channel targeting SARS-CoV-2 positive-sense (genomic) RNA and 20-ZZ ISH probes (845701, negative-sense RNA probe 1) with C1 channel targeting SARS-CoV-2 negative-sense (replicative intermediate) RNA were designed and synthesized by Advanced Cell Diagnostics (Supplemental Table 2). Tissue sections were deparaffinized with xylene, underwent a series of ethanol washes and peroxidase blocking, and were then heated in kit-provided antigen retrieval buffer and digested by kit-provided proteinase. Sections were exposed to ISH target probe pairs and incubated at 40°C in a hybridization oven

for 2 hours. After rinsing, ISH signal was amplified using kit-provided pre-amplifier and amplifier conjugated to alkaline phosphatase and incubated with a fast red substrate solution for 10 minutes at room temperature. Sections were then stained with hematoxylin, air dried, mounted, and stored at 4°C until image analysis.

mFISH. mFISH was performed using the RNAscope Fluorescent Multiplex Kit (Advanced Cell Diagnostics) according to the manufacturer's instructions, with minor modifications. In addition to positive-sense RNA probe 1 (red), another 40-ZZ probe with C3 channel (green, 854851-C3, negative-sense RNA probe 2) targeting negative-sense (replicative intermediate) SARS-CoV-2 RNA was designed and synthesized by Advanced Cell Diagnostics (Supplemental Table 2). FFPE tissue sections underwent deparaffinization with xylene and a series of ethanol washes and treatment with 0.1% Sudan Black B (MilliporeSigma) to reduce autofluorescence. Tissues were heated in kit-provided antigen retrieval buffer and digested by kit-provided proteinase. Sections were exposed to mFISH target probes and incubated at 40°C in a hybridization oven for 2 hours. After rinsing, mFISH signal was amplified using company-provided pre-amplifier and amplifier conjugated to fluorescent dye. Sections were counterstained with DAPI (Thermo Fisher Scientific), mounted, and stored at 4°C until image analysis. mFISH images were captured on an LSM 880 confocal microscope (Zeiss) and processed using ImageJ.

Dual staining. Subsequent to the fast red substrate reaction step of the ISH procedure using positive-sense RNA probe 2 (Supplemental Table 2) without any other pretreatment (antigen retrieval was performed during previous RNAscope ISH procedures as detailed in the kit manufacturer's instructions), sections were covered with a 1:250 dilution of rabbit polyclonal anti-SARS-CoV S antibody (Sino Biological, 40150-T62-COV2; Supplemental Table 1) overnight at 4°C. The next morning, sections were rinsed, and the peroxidase-labeled polymer (secondary antibody) was applied for 45 minutes. Slides were rinsed, and a brown chromogenic substrate, DAB solution (Dako Agilent Pathology Solutions), was applied for 8 minutes. Sections were then stained with hematoxylin, air dried, mounted, and stored at 4°C until image analysis.

Study approval. Study approval was not required for this study, because neither animal studies nor human samples were used.

Author contributions

XZ conceived and designed the experiments. JL, AMB, BJK, SRR, and XZ performed experiments. SRR, JHK, and XZ interpreted the data and wrote the manuscript with input from all authors.

Acknowledgments

We thank Lynda Miller and Neil Davis (USAMRIID) for histology assistance and Paul Facemire and Kathleen Gibson (USAMRIID) for coordinating the cell infection study. This work was funded by Defense Health Program (DHP). JHK's participation was funded, in part, through a Laulima Government Solutions LLC prime contract with the NIAID under contract HHSN272201800013C. JHK performed this work as an employee of Tunnell Government Services (TGS), a subcontractor of Laulima Government Solutions LLC, under contract HHSN272201800013C. The views and conclusions contained in this document are those of the authors and should not be interpreted as necessarily representing the official policies, either expressed or implied, of the US Department of the Army, the US Department of Defense, the US Department of Health and Human Services, or of the institutions and companies affiliated with the authors. In no event shall any of these entities have any responsibility or liability for any use, misuse, inability to use, or reliance upon the information contained herein. The US departments do not endorse any products or commercial services mentioned in this publication.

Address correspondence to Xiankun Zeng, United States Army Medical Research Institute of Infectious Diseases (USAMRIID), 1425 Porter Street, Fort Detrick, Frederick, Maryland 21702, USA. Phone: 301.619.3401; Email: xiankun.zeng.ctr@mail.mil.

1. Wu F, et al. A new coronavirus associated with human respiratory disease in China. *Nature*. 2020;579(7798):265–269.
2. Zhou P, et al. A pneumonia outbreak associated with a new coronavirus of probable bat origin. *Nature*. 2020;579(7798):270–273.
3. Zhu N, et al. A novel coronavirus from patients with pneumonia in China, 2019. *N Engl J Med*. 2020;382(8):727–733.
4. World Health Organization. WHO Coronavirus Disease (COVID-19) Dashboard. <https://covid19.who.int/>. Accessed May 21, 2020.
5. Lu R, et al. Genomic characterisation and epidemiology of 2019 novel coronavirus: implications for virus origins and receptor binding. *Lancet*. 2020;395(10224):565–574.

6. *Coronaviridae* Study Group of the International Committee on Taxonomy of Viruses. The species severe acute respiratory syndrome-related coronavirus: classifying 2019-nCoV and naming it SARS-CoV-2. *Nat Microbiol.* 2020;5(4):536–544.
7. Hoffmann M, et al. SARS-CoV-2 cell entry depends on ACE2 and TMPRSS2 and is blocked by a clinically proven protease inhibitor. *Cell.* 2020;181(2):271–280.e8.
8. Drexler JF, Corman VM, Drosten C. Ecology, evolution and classification of bat coronaviruses in the aftermath of SARS. *Antiviral Res.* 2014;101:45–56.
9. Paraskevis D, Kostaki EG, Magiorkinis G, Panayiotakopoulos G, Sourvinos G, Tsioupras S. Full-genome evolutionary analysis of the novel corona virus (2019-nCoV) rejects the hypothesis of emergence as a result of a recent recombination event. *Infect Genet Evol.* 2020;79:104212.
10. Ong SWX, et al. Air, surface environmental, personal protective equipment contamination by severe acute respiratory syndrome coronavirus 2 (SARS-CoV-2) from a symptomatic patient. *JAMA.* 2020;323(16):1610–1612.
11. van Doremalen N, et al. Aerosol and surface stability of SARS-CoV-2 as compared with SARS-CoV-1. *N Engl J Med.* 2020;382(16):1564–1567.
12. Yang X, et al. Clinical course outcomes of critically ill patients with SARS-CoV-2 pneumonia in Wuhan, China: a single-centered, retrospective, observational study. *Lancet Respir Med.* 2020;8(5):475–481.
13. Guan WJ, et al. Clinical characteristics of coronavirus disease 2019 in China. *N Engl J Med.* 2020;382(18):1708–1720.
14. Xu XW, et al. Clinical findings in a group of patients infected with the 2019 novel coronavirus (SARS-Cov-2) outside of Wuhan, China: retrospective case series. *BMJ.* 2020;368:m606.
15. Bhatraju PK, et al. Covid-19 in critically ill patients in the Seattle region — case series [published online March 30, 2020]. *N Engl J Med.* <https://doi.org/10.1056/NEJMoa2004500>.
16. Zhang H, et al. Histopathologic changes SARS-CoV-2 immunostaining in the lung of a patient with COVID-19. *Ann Intern Med.* 2020;172(9):629–632.
17. Xu Z, et al. Pathological findings of COVID-19 associated with acute respiratory distress syndrome. *Lancet Respir Med.* 2020;8(4):420–422.
18. Luo W, et al. Clinical pathology of critical patient with novel coronavirus pneumonia (COVID-19) [preprint]. <https://www.preprints.org/manuscript/202002.0407>. Posted on Preprints February 27, 2020.
19. Bao L, et al. The pathogenicity of SARS-CoV-2 in hACE2 transgenic mice [published online May 7, 2020]. *Nature.* <https://doi.org/10.1038/s41586-020-2312-y>.
20. Shi J, et al. Susceptibility of ferrets, cats, dogs, and other domesticated animals to SARS–coronavirus 2 [published online April 8, 2020]. *Science.* <https://doi.org/10.1126/science.abb7015>.
21. Kim Y-I, et al. Infection rapid transmission of SARS-CoV-2 in ferrets. *Cell Host Microbe.* 2020;27(5):704–709.e2.
22. Chan JFW, et al. Simulation of the clinical and pathological manifestations of coronavirus disease 2019 (COVID-19) in golden Syrian hamster model: implications for disease pathogenesis and transmissibility [published online March 26, 2020]. *Clin Infect Dis.* <https://doi.org/10.1093/cid/ciaa325>.
23. Deng W, et al. Ocular conjunctival inoculation of SARS-CoV-2 can cause mild COVID-19 in Rhesus macaques [preprint]. <https://doi.org/10.1101/2020.03.13.990036>. Posted on bioRxiv March 30, 2020.
24. Munster VJ, et al. Respiratory disease and virus shedding in rhesus macaques inoculated with SARS-CoV-2 [published online May 12, 2020]. *Nature.* <https://doi.org/10.1038/s41586-020-2324-7>.
25. Rockx B, et al. Comparative pathogenesis of COVID-19, MERS and SARS in a non-human primate model [published online April 17, 2020]. *Science.* <https://doi.org/10.1126/science.abb7314>.
26. Zeng X, et al. Identification and pathological characterization of persistent asymptomatic Ebola virus infection in rhesus monkeys. *Nat Microbiol.* 2017;2:17113.
27. Cashman KA, et al. Immune-mediated systemic vasculitis as the proposed cause of sudden-onset sensorineural hearing loss following Lassa virus exposure in cynomolgus macaques. *mBio.* 2018;9(5):e01896-18.
28. Coffin KM, et al. Persistent Marburg virus infection in the testes of nonhuman primate survivors. *Cell Host Microbe.* 2018;24(3):405–416.e3.
29. Liu J, et al. Nipah virus persists in the brains of nonhuman primate survivors. *JCI Insight.* 2019;4(14):e129629.
30. Shieh WJ, et al. Immunohistochemical, in situ hybridization, and ultrastructural localization of SARS-associated coronavirus in lung of a fatal case of severe acute respiratory syndrome in Taiwan. *Hum Pathol.* 2005;36(3):303–309.
31. Martinez RB, Ng DL, Greer PW, Rollin PE, Zaki SR. Tissue and cellular tropism, pathology and pathogenesis of Ebola and Marburg viruses. *J Pathol.* 2015;235(2):153–174.
32. Gary JM, et al. Lassa virus targeting of anterior uvea and endothelium of cornea and conjunctiva in eye of guinea pig model. *Emerging Infect Dis.* 2019;25(5):865–874.
33. Wang F, et al. RNAscope: a novel in situ RNA analysis platform for formalin-fixed, paraffin-embedded tissues. *J Mol Diagn.* 2012;14(1):22–29.
34. van der Eijk AA, et al. Miscarriage associated with Zika virus infection. *N Engl J Med.* 2016;375(10):1002–1004.
35. Cooper TK, et al. Histology, immunohistochemistry, and in situ hybridization reveal overlooked Ebola virus target tissues in the Ebola virus disease guinea pig model. *Sci Rep.* 2018;8(1):1250.
36. Smith DR, et al. Persistent Crimean-Congo hemorrhagic fever virus infection in the testes and within granulomas of non-human primates with latent tuberculosis. *PLoS Pathog.* 2019;15(9):e1008050.
37. de Wit E, van Doremalen N, Falzarano D, Munster VJ. SARS and MERS: recent insights into emerging coronaviruses. *Nat Rev Microbiol.* 2016;14(8):523–534.
38. Rhodes A, et al. A formalin-fixed, paraffin-processed cell line standard for quality control of immunohistochemical assay of HER-2/neu expression in breast cancer. *Am J Clin Pathol.* 2002;117(1):81–89.
39. Knudsen BS, et al. A novel multipurpose monoclonal antibody for evaluating human c-Met expression in preclinical and clinical settings. *Appl Immunohistochem Mol Morphol.* 2009;17(1):57–67.